ORIGINAL RESEARCH ARTICLE

Microstructure and Deposition Mechanism of Suspension Plasma Spraying Thermal Barrier Coatings

Zhongyu Zhu, Chaohui Wang, You Wang, Xiaodong Zhang, Wei Lin, Meiling Dong, Yuan You, Cheng Weidong, Jiaqi Liu, and Yuhang Wang

Nanostructured ceramic coatings are a promising research hotspot in the field of thermal protection coatings. Suspension plasma spraying is a practical thermal spaying technique to produce nanostructured thermal barrier coatings. In this paper, nanostructured 8YSZ (8 wt.% yttria-stabilized zirconia) thermal barrier coatings were fabricated using feedstocks of nano-8YSZ suspension by suspension plasma spraying, which was improved from air plasma spraying equipment attached to the atomizer feedstock device. Coatings microstructural analysis and testing were carried out by scanning electron microscope (SEM), and porosity was measured in cross-sectional SEM micrograph. The single scanning deposition status of 8YSZ coatings was investigated, analyzing SEM micrographs of single scanning coatings using different process parameters that included other solvents and additional locations in the plasma jet. The results show that deposition efficiency is higher using alcohol as a solvent, and a better melting state existed in the middle of the plasma jet. The cross-sectional microstructures in different thickness coatings were comparatively researched. More defects were observed in the microstructure of thicker coating, which can be produced by more residual thermal stress. This dramatically improves the thermal cycling performance of the coating.

1. Introduction

Because of the higher combustion temperature of the new generation of aircraft turbine engines, the heat resistance of component materials has higher requirements (Ref 1). Thermal barrier coatings (TBCs) have been developed for metal parts (such as combustion chamber inner walls and turbine blades.) that can endure higher temperatures while improving engine performance (Ref 2). In accordance with this purpose, thermal barrier coatings (TBCs) are used to increase the lifetime of gas turbine engine components that have not reached desired levels yet (Ref 3). Thermal barrier coatings (TBCs) are protective coating systems that are mostly utilized to improve the thermal insulation and functional performance of gas turbine engines and other aircraft components that are both stable and movable (Ref 4-7). Thermal Barrier Coatings (TBCs) are generally used in both industrial gas turbines and aircraft engines (Ref 8-10). Thermal barrier coatings (TBCs) are used to protect metallic

Zhongyu Zhu, Chaohui Wang, You Wang, Xiaodong Zhang, Wei Lin, Meiling Dong, Yuan You, Cheng Weidong, and **Jiaqi Liu**, Heilongjiang Provincial Key Laboratory of Polymeric Composite Materials, College of Materials Science and Engineering, Qiqihar University, Qiqihar, People's Republic of China; and **Yuhang Wang**, Heilongjiang Provincial Key Laboratory of Polymeric Composite Materials, College of Materials Science and Engineering, Qiqihar University, Qiqihar, People's Republic of China; and College of Materials Science and Engineering, Harbin Institute of Technology, Harbin, Heilongjiang, China. Contact e-mail: wch800209@126.com.

components of gas turbines against such failures (Ref 11). The following techniques were used to prepare thermal barrier coatings: electron beam-physical vapor deposition (EB-CVD) (Ref 12-14), chemical vapor deposition (CVD) (Ref 15), the cold gas dynamic spray (CGDS) (Ref 16), and plasma spraying (PS) methods. The PS and EB-PVD were necessary procedures in this field of TBCs (Ref 17, 18). PS techniques include vacuum plasma spraying (VPS), low-pressure plasma spraying (LPPS), atmospheric plasma spraying (APS), and liquid-phase thermal spraying (LPS) (Ref 19-21).

In recent years, liquid-phase thermal spraying technology has been well-known by engineering researchers, especially in the field of nano/submicron surface engineering, which has achieved efficient nano-coatings by liquid-phase thermal spraying technology and applied to many new research areas [22]. Liquid-phase spraying is a new type of technology of coating prepared by liquid-phase feedstocks through a new feeding device on the original thermal spraying equipment. The liquid-phase material was mainly used as the carrier of coating materials and was heated into the gas phase during thermal spraying. The suspended materials or solutes in the liquid phase, with the evaporation of the liquid solvent, were physically transformed into small particles and aggregated. Unique feedstocks were deposited on the substrates, forming coatings with unique structures. This method was used in this study; various layers were prepared in previous papers. Stefan Kozerski et al. (Ref 23) prepared thermal barrier coatings of micron powder YSZ suspensions by suspension plasma spraying with a suitable adhesive interface between the layer and the substrate (Ref 24, 25). Bacicini et al. (Ref 26) presented YSZ coatings with typical nanostructures using liquid-phase thermal spraying with an average grain size of 50 nm. Fauchais P et al. (Ref 27) showed that YSZ coatings by liquid-phase thermal spraying have better thermal shock properties than YSZ coatings by powder plasma spraying. The lower crack density

can be seen by microscopic characterization, and longitudinal cracks were shown in the coatings prepared by liquid-phase thermal spraying after thermal shock (Ref 28). These longitudinal cracks effectively dispersed the thermal stresses generated during the thermal shock process. In this paper, nanostructured 8YSZ thermal barrier coatings with nanostructure were prepared by suspension plasma spraying with nano-YSZ suspension feedstocks, focusing on the process parameters.

2. Experimental

The GH4169 high-temperature alloy was selected as substrate material, made into $\Phi20 \times 6$ disks, which were cleaned with acetone and sandblasted before spraying. NiCoCrAlY bonding coating, about 50-80 μm, was spread by conventional atmospheric plasma spraying. The top ceramic coatings of the thermal barrier coating system were prepared by suspension plasma spraying. The suspension feedstocks were suspensions of ceramic powders dispersed in an alcohol medium, which were injected into the plasma jet of the plasma spraying. The main process parameters of the plasma spraying equipment in the suspension plasma spraying process are shown in Table 1.

The solid phase content of the nano-powder in the nano-powder suspension was about 30-50 wt.%. The ball milling media in the stirred ball milling process were zirconia balls of $\Phi20$, $\Phi10$, and $\Phi5$, which were graded according to the weight ratio of 3:4:3. The speed of the stirred ball mill was 60 rpm, the dispersion medium was alcohol or deionized water, PEG1000 was added, and the ball milling time was 4-24 h. The temperature of the suspension during ball milling did not exceed 40 °C. After ball milling and filtering through a 300 mesh sieve, the slurry was placed in a sealed sample and set aside. The prepared suspensions need to be free of significant stratification within 24 hours. The rest should be stirred with a mechanical stirrer to avoid the soft agglomeration and precipitation of the nano-powders.

The microscopic morphologies of the raw materials and plasma sprayed coatings were analyzed by optical microscope (MC 80DX, Carl Zeiss, Germany) and scanning electron microscope (SEM, S-3400, Hitachi, Japan), respectively. When analyzing the surface morphology of thermal spraying raw materials by SEM, the sprayed powder was dispersed uniformly on the conductive adhesive and gold-sprayed. When analyzing the microstructure of the coating surface by SEM, the scattered specimens were cleaned with ultrasonic alcohol and sprayed with gold. When analyzing the cross-sectional microscopies of the coatings, the process of sample preparation is as follows: the sprayed coating specimen was vertically cut by diamond wire saws to make a cross-sectional specimen. The specimens were embedded into epoxy resin to expose only the cross section and ground and polish (Fig. 1).
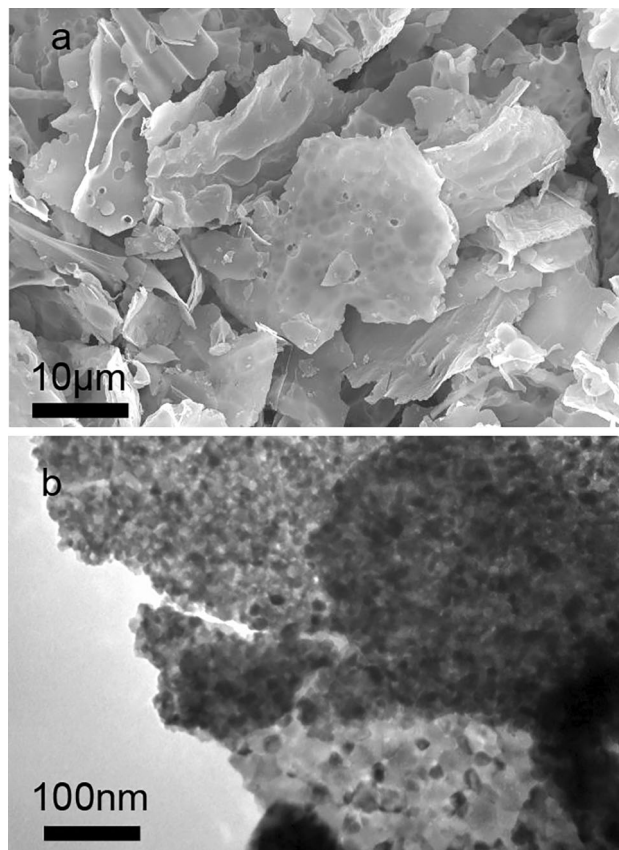
Fig. 1 (a) SEM and (b) TEM images of nanosized 8YSZ feedstocks

The physical phases of the sprayed powders and coatings were analyzed using an x-ray diffractometer (XRD) (D8 manufactured by BRUKER-AXS, Germany) with copper target Kα rays (λ = 1.5418 Å), graphite monochromator filter, scanning speed of 10°/min, step size of 0.02°, accelerating voltage of 40KV, current of 100 mA. XRD theta-2theta scanning was carried out in the plane normal to the sample surfaces with a 2theta-angle range between 20° and 80° with a scanning speed of 40 min^{-1}. The approximate grain sizes of the nanostructured material under test were analyzed using XRD diffraction patterns, and the grain size D was calculated by the Scherrer equation (Ref 29, 30) (1).

$$\mathbf{D} = \mathbf{k}\lambda/\beta\mathbf{cos}\theta \qquad (\text{Eq 1})$$

where: D—average width in the direction of the vertical crystal plane. λ—the wavelength. β—diffraction peak half-height width (FWHM). θ—the diffraction angle. K—constant, taken as 0.89.

Thermal shock resistance of thermal barrier coatings refers to the ability of the layers to resist thermal stress and avoid cracking and peeling during the course of repeated heating-

Table 1 Suspension plasma spraying process parameters

Current, A	Voltage, V	Fogging pressure, bar	Feeding rate, ml·min^{-1}	Spray gun speed, m·s^{-1}
650	60	0.1–1	10–20	0.5–2

cooling alternating changes. The thermal shock resistance of the thermal barrier coating was tested by referring to the Japanese Industrial Standard JIS 8666-1990 (Ref [20]). The temperature of the furnace was set at 1000 °C. When the furnace was raised to the set temperature, the test specimen was placed into the middle of the stove. After the illustration endured in the furnace for 5 min, they were quickly removed and quenched in room temperature water, dried with an electric hand dryer, and observed with a magnifying lens to observe cracks, flaking, and peeling on the surface. A digital camera was taken pictures of thermal barrier coatings after each thermal cycle, and the mass value of the specimen was weighed on an analytical balance (Suture BSA224, Suture Scientific Instruments (Beijing) Co., Ltd., Beijing, PR China). After cooling, the specimens were put into the resistance furnace again. Repeating the thermal shock cycle until the area of cracks, peeling, and flaking of the coating accounts for more than 20% of the whole coating area, the layer is considered to be invalid, and the thermal shock test is terminated.

3. Results and Discussion

3.1 Parameters of SPS for YSZ Coatings

3.1.1 Feed Atomization. In this research, suspension as the thermal spraying feed was atomized by twin-fluid atomizer which was assembled on the plasma spray torch. The atomization status of suspension contained 30 wt.% of 8YSZ solid phase is shown in Fig. 2. Suspension was deformed into a cone under high-pressure air driven and static air impeded. Here, the droplets are divided into three parts and have different shapes. At the midline of the cone, the mist droplets are almost spherical.

From the comparison of the SEM analysis results, as the concentration increases, the atomized particles increase and the spread area of deposition after spraying increases gradually, but after reaching a certain level, the spread area of individual particles decreases which indicates that the oversized droplets will break into small pieces under the impact of the plasma airflow instead. From the point of view of deposited particles, at low feeding speeds, the number of deposited particles formed is small because the tiny droplets formed do not gain enough kinetic energy to enter the plasma and the flame edge temperature is not sufficient to evaporate and melt the solid phase particles. When the feeding speed is increased, the particles of the suspension atomization are significantly increased, and the kinetic energy and momentum obtained are greatly increased to enter the interior of the plasma flame stream. Under the action of high temperature and thermal energy, the dispersed medium in the suspension droplets can be rapidly evaporated and the remaining solid phase in the droplets can be rapidly warmed up and deposited on the surface of the substrate to form a coating under the impetus of the plasma flame stream. From the point of view of deposited particles, when the feeding speed is low, the number of deposited particles formed is small because the small droplets formed do not gain enough kinetic energy to enter the plasma and the temperature at the flame edge is not sufficient to evaporate and melt the solid phase particles. When the feeding speed is increased, the particles after atomization of the suspension are greatly increased, and the kinetic energy and momentum obtained are greatly increased to enter the interior of the plasma flame stream, and under the action of high temperature and thermal energy, the dispersed medium in the suspension droplets can be rapidly evaporated and the remaining solid phase in the droplets can be rapidly warmed up and deposited
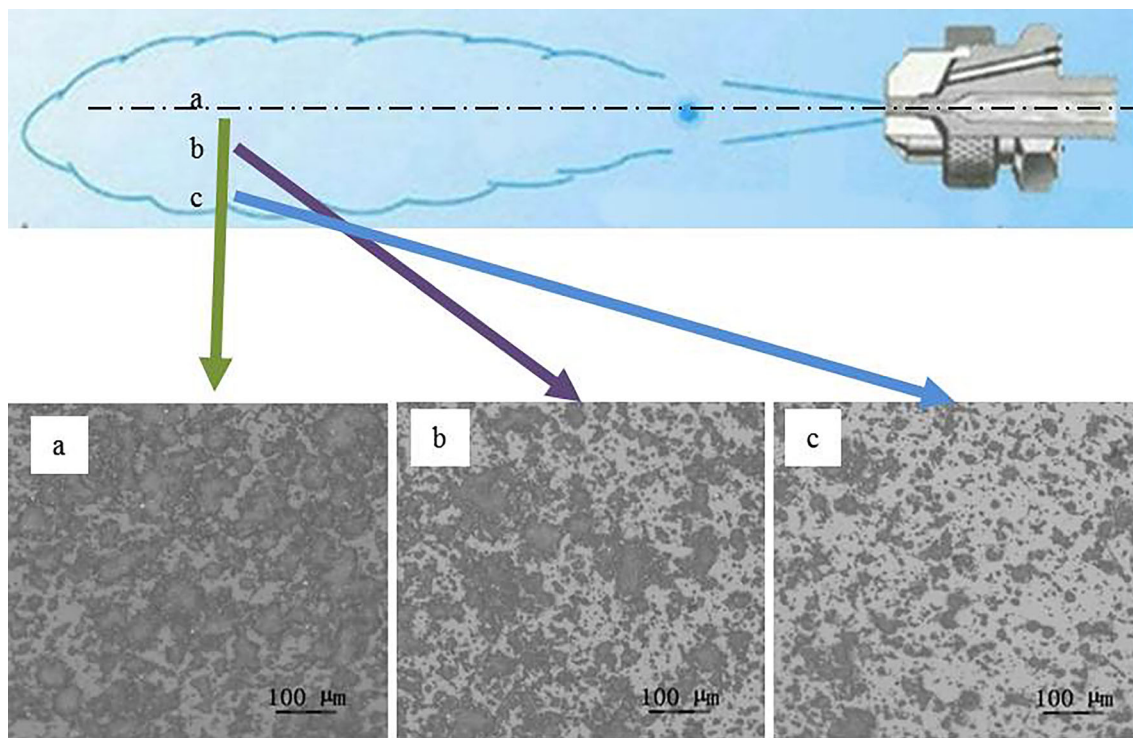
Fig. 2 Atomization status at (a) center, (b) near center, (c) margin of beam during the feed of suspension thermal spraying

on the surface of the substrate to form a coating under the impetus of the plasma flame stream. It can be seen from the figure that when the feeding rate reaches a feed rate of 21 ml/min, a typical spray deposit state is formed, and a good bond is formed. The greater the feed rate, the higher the efficiency of the spraying, so 21 ml/min was chosen as the feed rate parameter after optimization.

3.1.2 Solvent of Suspension. In SPS, suspension feedstocks are different from powders feedstocks in APS. Suspension is composed of solvent and solid particles. The solid particles can be deposited on the matrix to fabricate the coatings. And solvent can be acted as a carrier of fine particles and improve the liquidity of feedstocks. However, solvent would consume thermal energy and influence deposition of coatings. Water is one of the commonly used leaching solvents, which is economical and easy to obtain, with high polarity, wide solubility range and strong safety, and can be mixed with ethanol, glycerol, and other polar solvents. Compared with water, ethanol has small specific heat, low boiling point and small latent heat of vaporization, so it consumes less heat than water in the process of evaporation and concentration of leaching solution. Common solvents are selected to justify the choice of suspensions. In Fig. 3, three kinds of solvents were selected, which were full water, 50 wt.% water + 50 wt.% alcohol and full alcohol. The existence of water increased energy consumption in solvent due to its higher evaporation enthalpy than alcohol. It can be seen in Fig. 4, with less water in the solvent, molten particles decreased significantly, because the value of water vaporization heat is bigger than alcohol vaporization heat, the vaporization heat of water is 2257.2 kJ/kg at the temperature of evaporation point 100 °C, and

vaporization heat of alcohol is 855 kJ/kg at temperature of evaporation temperature 78.3 °C. In the process of SPS, liquid-phase evaporation consumes a lot of heat and leads to insufficient heat. Therefore, alcohol is more suited for the liquid media of suspension in the SPS process.

3.1.3 Scanning Times. The scanning speed of plasma torch was uniformly 1 m/s in this paper, and the thickness of the coating was controlled by scanning times. From Fig. 5, the conclusion can be drawn out that the deposition rate of SPS was about 1um per scanning. The deposition rate slightly increased when scanning time was prolonged to fabricate thicker coatings. In Fig. 5(a) and (b), the cross-sectional microscopies of YSZ coatings were uniform with porosity (about 7%). In Fig. 5(c), vertical and horizontal cracks can be seen in the cross section, which can be due to the more residual stress existing in the thicker coating. Therefore, the coating thickness of coatings fabricated by SPS should be controlled under 300um.

### 3.2 Deposition Mechanics of Suspension Plasma Spraying

Suspension feedstocks were different from Conventional air plasma spray in the process of suspension plasma spray. Fig. 6 shows the process mechanism that suspension evolved from liquid to coating. Suspensions firstly were atomized in two-flow atomizing nozzle into droplets which sizes were 60-80 μm in accordance with feedstock sizes of APS. Fog drops were injected into the plasma jet under the drive of the airflow from the atomizing nozzle. Solvents in suspension fog drops were evaporated, which led to aggregation and partly sintering of nanoparticles in suspension. Then, the outside surface of the aggregation partly melted. At last, the aggregation with melt hit specimen surface to form deposition coatings.
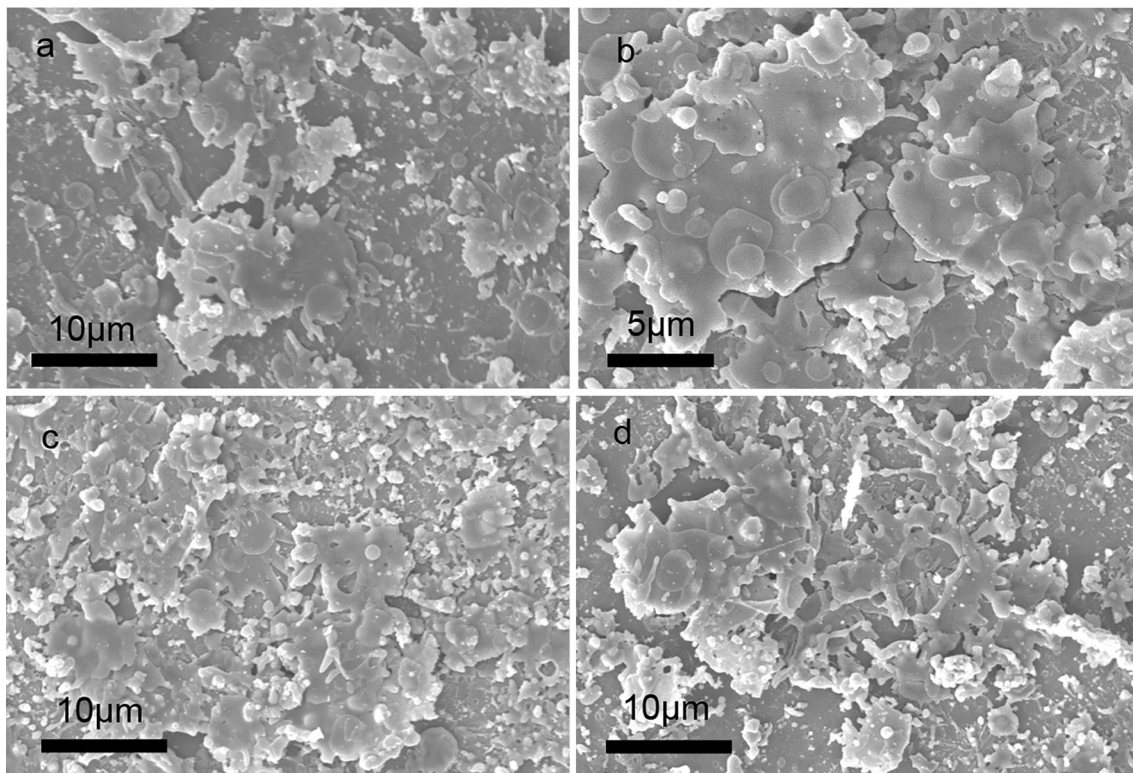
Fig. 3 SEM images of single scanning of coatings fabricated by different feed rates (a) 16 ml/min; (b) 21 ml/min; (c) 27 ml/min; (d) 31 ml/min
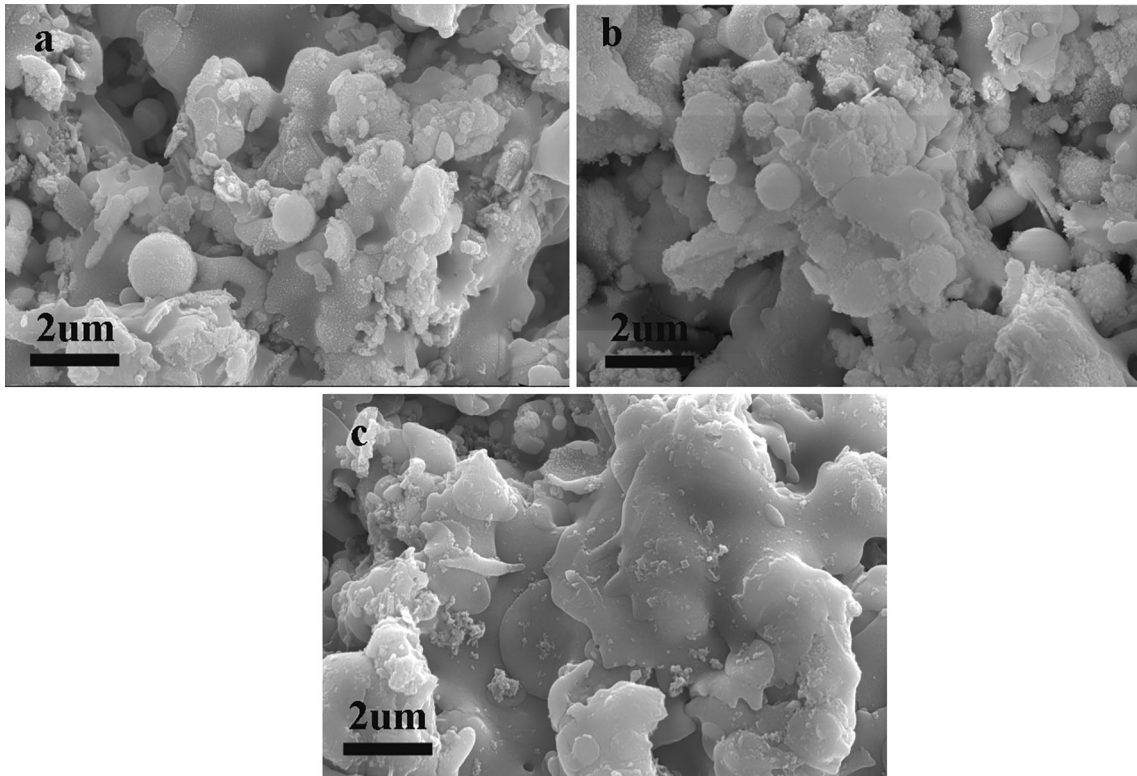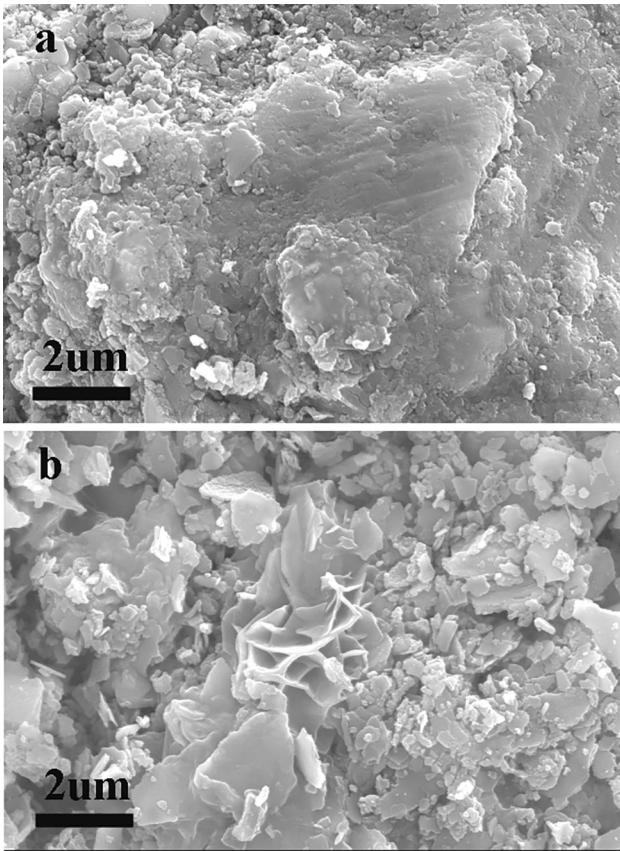
Fig. 4 Surface images of coatings used suspensions of different solvents (a) water; (b) 50 wt.% water + 50 wt.% alcohol; (c) alcohol
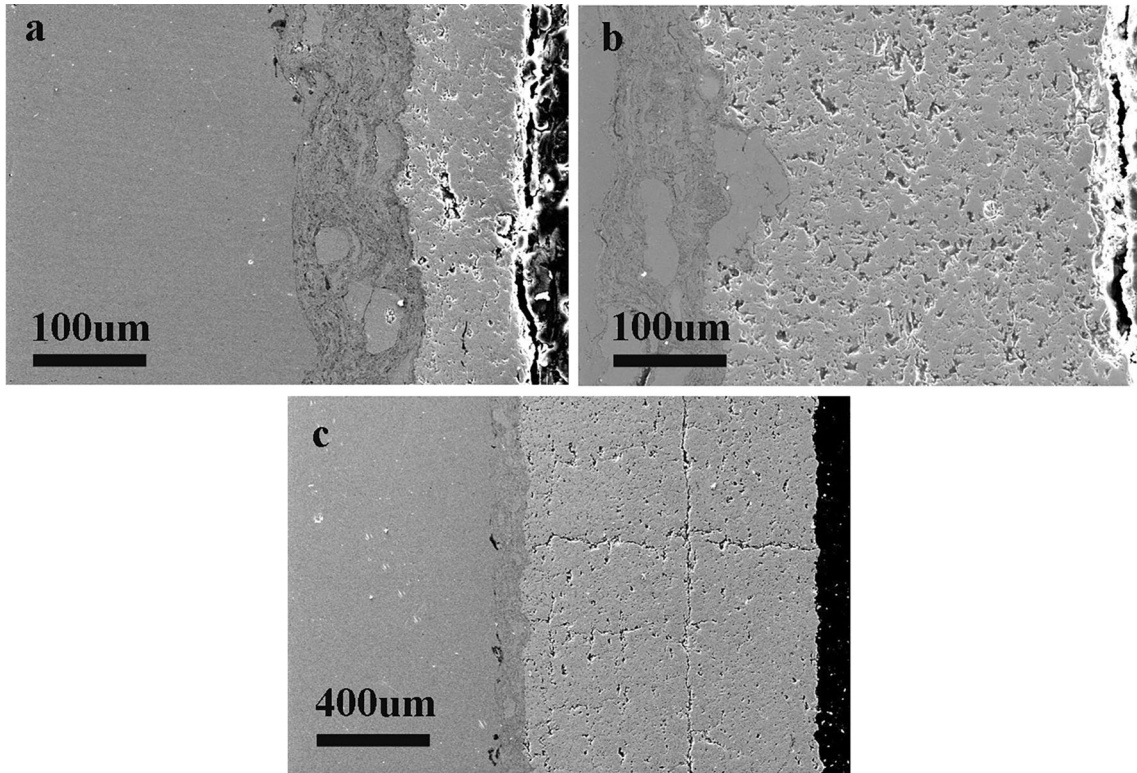
Fig. 5 Cross-sectional SEM images of 8YSZ coatings fabricated by scanning speed 1 m/s and different scanning times (a) 150 times (120um thickness); (b) 300 times (300 um thickness); (c) 900 times (960 um thickness)

Fig. 6 Mechanism analysis of SPS process

### 3.3 The Surface Microscopy of the YSZ Coatings

SEM images of coatings surface are shown in Fig. 7. Surface morphology of the coatings by suspension plasma spraying is like that of coatings by ordinary atmospheric plasma spraying with layered structure. The diagram shows that this is a surface structure formed by the accumulation of particles. However, finer microstructure can be found in the surface morphology of the coating produced by suspension plasma spraying in comparison with conventional atmospheric plasma spraying. In Fig. 7(a), in low-magnification SEM image, average diameter size of the splats is about 70-80 microns. And in Fig. 7(b), SEM images at magnification 2000 × , it can be shown that the deposited structure of droplets is very tight with some micropores, which are very small about 1 um. The SEM images were converted into black and white two-bit images using Image-Pro Plus software. The number of pixels in the white part was sampled and counted, and the number of pixels divided by the total number of pixels in the whole image was the porosity. Fig. 7(c) magnification 10,000 ×, little droplets about 2 μm were deposited on former deposited splats, and all surfaces were composed of nanosized fine spheres ($\sim$100 nm) which caused a lot of interface defects in microstructure of coatings. These obvious interfaces greatly improved the thermal insulation efficiency of thermal barrier coating, and those also had a significant obstacle on the crack propagation lead to improve the thermal shock resistance of coatings.

3.4 XRD Analysis

The XRD patterns show that the as-sprayed coatings and the feedstocks are composed of $((ZrO_2)_{0.92}(Y_2O_3)_{0.08})_{0.926}$ tetragonal zirconia phases according to PDF#70-4431 in Fig. 8. The
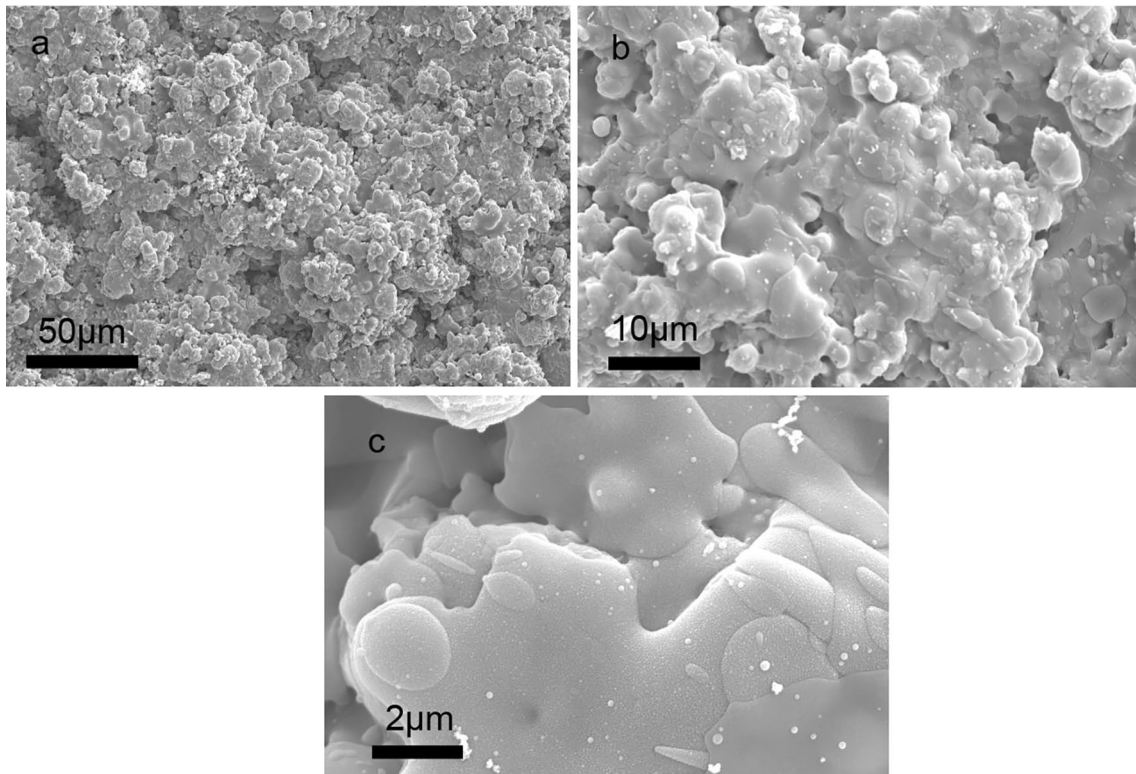
Fig. 7 Scanning electron microscope images of coating surfaces at different magnifications: (a) 500×, (b) 2000× , (c) 10000 ×
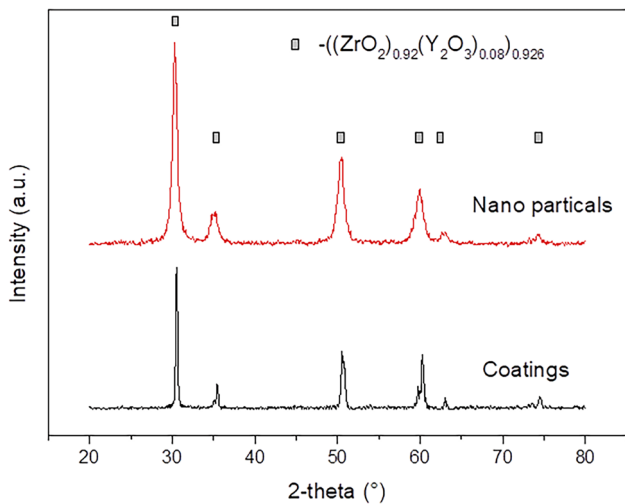
Fig. 8 XRD patterns of nanoparticles and coatings of YSZ

grain size of as-sprayed coatings determined by the Scherrer equation is 45 nm, and that of feedstocks is 28 nm. Although the average grain size grew obviously, the grain size of as-sprayed coatings remained at the nanometer scale.

3.5 Thermal Shock Tests

The thermal shock cycle with water quenching was conducted in 1000 °C high-temperature furnace. The surface spallation area of the suspension plasma spraying coating reached 20% after 160 cycles, which was significantly higher than 50 cycles of the YSZ coating sprayed by atmospheric plasma spraying (Ref 26). The results were related to the nano-sized microstructure of coatings by suspension plasma spraying. There were a lot of grain boundaries in the nano-structured coatings, which could effectively absorb the energy generated from thermal stress due to thermal cycling. The photographs of the coating before and after thermal shock are shown in Fig. 9, in which the spallation locations of coating were mainly at the edges of the specimen. The spallation of the TBCs was caused by the concentration of thermal stress from the mismatch of thermal expansion between 8YSZ and matrix. The cross-sectional microstructure and surface microstructure of the coating after thermal shock failure are shown in Fig. 10. The development of longitudinal cracks in the coating can be seen in the cross-sectional microstructure, with a clear TGO on the adhesive layer where cracks are clearly deflected. Some block spallation and obvious cracks were found on the surface, seen in Fig. 10(b). The results show that the failure of the coating is caused by the growth of cracks in the coating, where the appearance of thermal stresses is the main reason for the appearance of cracks, along with the flaking of some weak bonded parts from the coating surface.
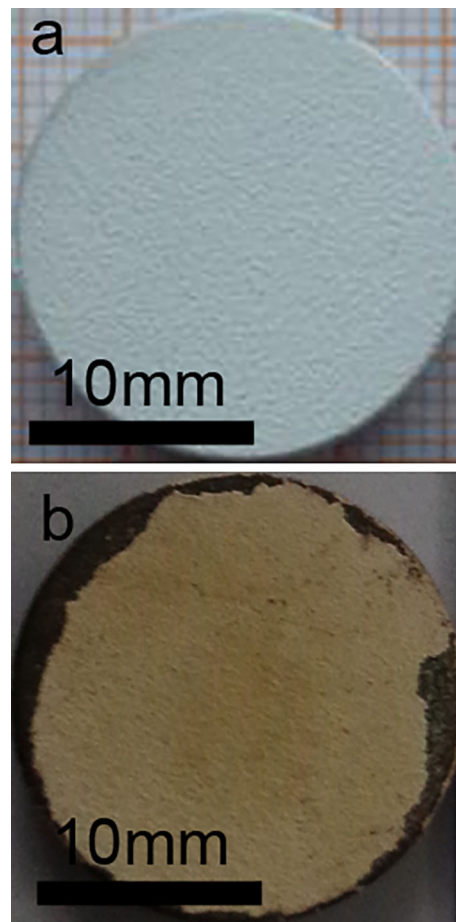

Fig. 9 Photos of specimens (a) as-sprayed YSZ coatings, (b) YSZ coatings after thermal shock tests

4. Conclusions

In this paper, 8YSZ thermal barrier coating was successfully prepared by suspension plasma spraying (Ref 31). Through the analysis of the coating preparation process and the research of coating properties, the following conclusions were concluded:

(1) Suspension plasma spraying process was mainly composed of suspension atomization, evaporation, sintering agglomeration, melting, impaction on the substrate to form a coating.
(2) Feeding speed, suspension dispersant and spraying time had an influence on the structure of the coating in the preparation process of the coating.
(3) Thermal cycling performance of the coating by suspension plasma spraying was better than that by air plasma spraying, the cracks propagation was the main reason
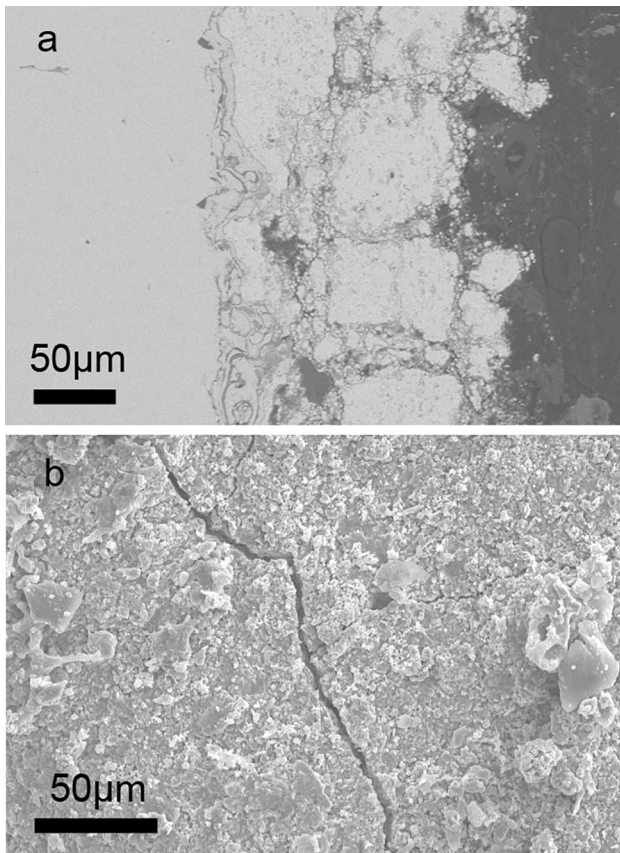
Fig. 10 Cross-sectional (a) and surface (b) SEM images of coatings after thermal shock tests

for the failure of the coating, and this significantly improved the thermal insulation efficiency of the thermal barrier coating, which also had a significant impact on crack extension and improved the thermal impact performance of the coating.

Acknowledgments

References

1. J.H. Perepezko, The Hotter the Engine, the Better, *Science*, 2009, **326**(5956), p 1068–1069.
2. N.P. Padture, M. Gell, and E.H. Jordan, Thermal Barrier Coatings for Gas-Turbine Engine Applications, *Science*, 2002, **296**(5566), p 280–284.
3. K.M. Doleker, A.C. Karaoglanli, Y. Ozgurluk, and A. Kobayashi, Performance of Single YSZ, $Gd_2Zr_2O_7$ and Double-Layered YSZ/ $Gd_2Zr_2O_7$ Thermal Barrier Coatings in Isothermal Oxidation Test Conditions, *Vacuum*, 2020, **177**, p 109401. https://doi.org/10.1016/j.vacuum.2020.109401
4. O. Odabas, Y. Ozgurluk, D. Ozkan et al., Investigation of Vermiculite Infiltration Effect on Microstructural Properties of Thermal Barrier Coatings (TBCs) Produced by Electron Beam Physical Vapor Deposition Method (EB-PVD), *Surf. Coat. Technol.*, 2022, **443**, p 128645.
5. K. Doleker, O. Mert, A. Yasin, K. Hayrettin, and C. Abdullah, Evaluation of Oxidation and Thermal Cyclic Behavior of YSZ, $Gd_2Zr_2O_7$ and YSZ/$Gd_2Zr_2O_7$ TBCs, *Surf. Coat. Technol.*, 2019, **371**, p 262.
6. M. Ozgurluk, Investigation of the Effect of V_2O_5 and Na_2SO_4 Melted Salts on Thermal Barrier Coatings under Cyclic Conditions, *Anti-Corros. Methods Mater.*, 2019, **66**(5), p 644–650.
7. K.M. Doleker, O. Odabas, Y. Ozgurluk et al., Effect of high Temperature Oxidation on Inconel 718 and Inconel 718/YSZ/ $Gd_2Zr_2O_7$, *Mater. Res. Express*, 2019, **6**(8), p 086456.
8. A. Yo, A. Ack, and B. Ha, Comparison of Calcium-Magnesium-Alumina-Silicate (CMAS) Resistance Behavior of Produced with Electron Beam Physical Vapor Deposition (EB-PVD) Method YSZ and Gd 2 Zr 2 O 7 /YSZ Thermal Barrier Coatings Systems, *Vacuum*, 2021, **194**, p 110576.
9. A. Yo, K.M. Doleker, C. Ha et al., Investigation of Calcium-Magnesium-Alumino-Silicate (CMAS) Resistance and Hot Corrosion Behavior of YSZ and $La_2Zr_2O_7$/YSZ Thermal Barrier Coatings (TBCs) Produced with CGDS Method, *Surf. Coat. Technol.*, 2021, **411**, p 126969.
10. Yasin Ozgurluk, Doleker, et al., Hot Corrosion Behavior of YSZ, $Gd_2Zr_2O_7$ and YSZ/$Gd_2Zr_2O_7$ Thermal Barrier Coatings Exposed to Molten Sulfate and Vanadate Salt, *Appl. Surf. Sci. A J. Devot. Propert. Interf. Relat. Synth. Behav. Mater.*, 2018, **438**(30), p 96–113.
11. M. Karaoglanli, Interface Failure Behavior of Yttria Stabilized zirconia (YSZ), $La_2Zr_2O_7$, $Gd_2Zr_2O_7$, YSZ/$La_2Zr_2O_7$ and YSZ/$Gd_2Zr_2O_7$ Thermal Barrier Coatings (TBCs) in Thermal Cyclic Exposure, *Mater. Characteriz.*, 2020, **159**, p 110072.
12. E. Lugscheider, K. Bobzin, S. Barwulf et al., Mechanical Properties of EB-PVD-Thermal Barrier Coatings by Nanoindentation, *Surf. Coat. Technol.*, 2001, **138**(1), p 9–13.
13. K.D. Bouzakis, A. Lontos, N. Michailidis et al., Determination of Mechanical Properties of Electron Beam-Physical Vapor Deposition-Thermal Barrier Coatings (EB-PVD-TBCs) by Means of Nanoindentation and Impact Testing, *Surf. Coat. Technol.*, 2003, **163**, p 75–80.
14. T. Goto, Thermal Barrier Coatings Deposited by Laser CVD, *Surf. Coat. Technol.*, 2005, **198**(1–3), p 367–371.
15. K.M. Doleker, Y. Ozgurluk, Y. Kahraman et al., Oxidation and Hot Corrosion Resistance of HVOF/EB-PVD Thermal Barrier Coating System, *Surface Coat. Technol.*, 2021, **409**, p 126862.
16. Y. Ozgurluk, K. Doleker, D. Ozkan et al., Cyclic Hot Corrosion Failure Behaviors of EB-PVD TBC Systems in the Presence of Sulfate and Vanadate Molten Salts, *Coatings*, 2019, **9**(3), p 166.
17. O.H. Ahlatci, Isothermal Oxidation Behavior of Gadolinium Zirconate ($Gd_2Zr_2O_7$) Thermal Barrier Coatings (TBCs) produced by Electron Beam Physical Vapor Deposition (EB-PVD) Technique, *Open Chem.*, 2018, **16**(1), p 986.
18. H.B. Guo, S.K. Gong, and H.B. Xu, Evaluation of Hot-Fatigue Behaviors of EB-PVD Gradient Thermal Barrier Coatings, *Mater. Sci. Eng. A-Struct. Mater. Propert. Microst. Process.*, 2002, **325**(1–2), p 261–269.
19. Karaoglanli AC, Ozgurluk Y, Doleker KM. (2020) Comparison of Microstructure and Oxidation Behavior of CoNiCrAlY Coatings Produced by APS, SSAPS, D-Gun, HVOF and CGDS Techniques. Vacu. Technol. Appl. Ion Phys. Int. J. Abstract. Service Vacu. Sci. Technol. 180: 109609
20. M. Kaplan, M. Uyaner, Y. Ozgurluk et al., Evaluation of Hot Corrosion Behavior of APS and HVOF Sprayed Thermal Barrier Coatings (TBCs) Exposed to Molten Na_2SO_4+V_2O_5 Salt at 1000°C, *Eng. Des. Appl.*, 2019, **444**, p 59.
21. K.M. Doleker, Y. Ozgurluk, A.S. Parlakyigit, D. Ozkan, T. Gulmez, and A.C. Karaoglanli, Oxidation Behavior of NiCr/YSZ Thermal Barrier Coatings (TBCs), *Open Chem.*, 2018, **16**(1), p 876–881. https://doi.org/10.1515/chem-2018-0096
22. R. Jaworski, L. Pawlowski, C. Pierlot et al., Recent Developments in Suspension Plasma Sprayed Titanium Oxide and Hydroxyapatite Coatings, *J. Therm. Spray Technol.*, 2010, **19**(1–2), p 240–247.
23. S. Kozerski, L. Łatka, L. Pawlowski et al., Preliminary Study on Suspension Plasma Sprayed ZrO_2+8wt.% Y_2O_3 Coatings, *J. Europ. Ceram. Soc.*, 2011, **31**(12), p 2089–2098.

24. R. Rampon, C. Filiatre, and G. Bertrand, Suspension Plasma Spraying of YPSZ Coatings: Suspension Atomization and Injection, *J. Therm. Spray Technol.*, 2008, **17**(1), p 105–114.

25. R. Jaworski, L. Pawlowski, F. Roudet et al., Characterization of Mechanical Properties of Suspension Plasma Sprayed TiO_2 Coatings Using Scratch Test, *Surf. Coat. Technol.*, 2008, **202**(12), p 2644–2653.

26. A. Bacciochini, G. Montavon, J. Ilavsky et al., Porous Architecture of SPS Thick YSZ Coatings Structured at the Nanometer Scale (Similar to 50 nm), *J. Therm. Spray Technol.*, 2010, **19**(1–2), p 198–206.

27. P. Fauchais and G. Montavon, Latest Developments in Suspension and Liquid Precursor Thermal Spraying, *J. Therm. Spray Technol.*, 2010, **19**(1–2), p 226–239.

28. H. Kassner, R. Siegert, D. Hathiramani et al., Application of Suspension Plasma Spraying (SPS) for Manufacture of Ceramic Coatings, *J. Therm. Spray Technol.*, 2008, **17**(1), p 115–123.

29. P. Zhang, A. Navrotsky, B. Guo et al., Energetics of Cubic and Monoclinic Yttrium Oxide Polymorphs: Phase Transitions, Surface Enthalpies, and Stability at the Nanoscale, *J. Phys. Chem. C*, 2008, **112**(4), p 932–938.

30. C.J. Wang, Y. Wang, Y.L. Cheng et al., Synthesis of Nanocrystalline La_2O_3-Y_2O_3-ZrO_2 Solid Solutions by Hydrothermal Method: A Crystal Growth and Structural Study, *J. Cryst. Growth*, 2011, **335**(1), p 165–171.

31. L. Wang, Y. Wang, X.G. Sun, J.Q. He, Z.Y. Pan, and C.H. Wang, Thermal Shock Behavior of 8YSZ and Double-Ceramic-Layer $La_2Zr_2O_7$/8YSZ Thermal Barrier Coatings Fabricated by Atmospheric Plasma Spraying, *Ceram Int.*, 2012, **38**, p 3595–3606.